Study of river flow based on finite element analysis and GPS-echo-sounder measurement

Hashentuya[1] Yoji Otani[2] Kazuhiro Yamamoto[3]
Masaji Watanabe[4]

(Received 31 January 2011; revised 15 February 2012)

Abstract

Currents of a river are analyzed numerically by introducing data concerning the water depth into a finite element analysis of the partial differential equations of the flow. Techniques to simulate currents generated in the river are described. The region is divided in the vertical direction into layers, and a finite element discretization in the horizontal direction is applied. Results of the simulation of flow generated in the Yoshii River in Okayama Prefecture of Japan are shown. We also introduce our techniques to measure the river bed topography using a hardware system consisting of a global positioning system and an echo sounder. Data obtained by using the system are introduced into the analysis of flow and corresponding numerical results are generated.

---

http://journal.austms.org.au/ojs/index.php/ANZIAMJ/article/view/3966 gives this article, Published March 7, 2012. ISSN 1446-8735.

Contents

1 Introduction **C1103**

2 Numerical solution by the finite element method **C1105**
2.1 Shallow water equations C1106
2.2 Initial condition C1107
2.3 Application to the multi-layer finite element method C1109
2.4 Time-step approximation C1115

3 Flow simulation downstream of the Kamogoshi Dam **C1118**

4 Conclusion **C1118**

References **C1123**

1 Introduction

Seto Inland Sea divides the main island and the Shikoku Island of Japan. The Yoshii River flows into the Kojima Bay which is connected to the Seto Inland Sea. It is one of three major rivers in Okayama Prefecture with $2,110\,\mathrm{km}^2$ basin area, $133\,\mathrm{km}$ length, and $61.16\,\mathrm{m}^3/\mathrm{s}$ average flow. Kamogoshi Dam is approximately $7\,\mathrm{km}$ upstream from the Yoshii River mouth and the latter is called Kuban. Water from upstream has been washing the riverbed in the area below the Kamogoshi Dam, and a deep water area has developed.

We analyze currents generated in the Yoshii River, downstream from the Kamogoshi Dam. The bottom topography is investigated by a global positioning system (GPS) and an echo sounder. Figure 1 shows the depth contours of the Yoshii River in the region near the Kamogoshii Dam. Note that the depth of the river ranges from $2\,\mathrm{m}$ to $9\,\mathrm{m}$. The depth data are based on GPS-echo-sounder measurements taken on March 14, 19, 22, 24, 29, and 30, 2010. Numerical results are obtained by introducing data concerning

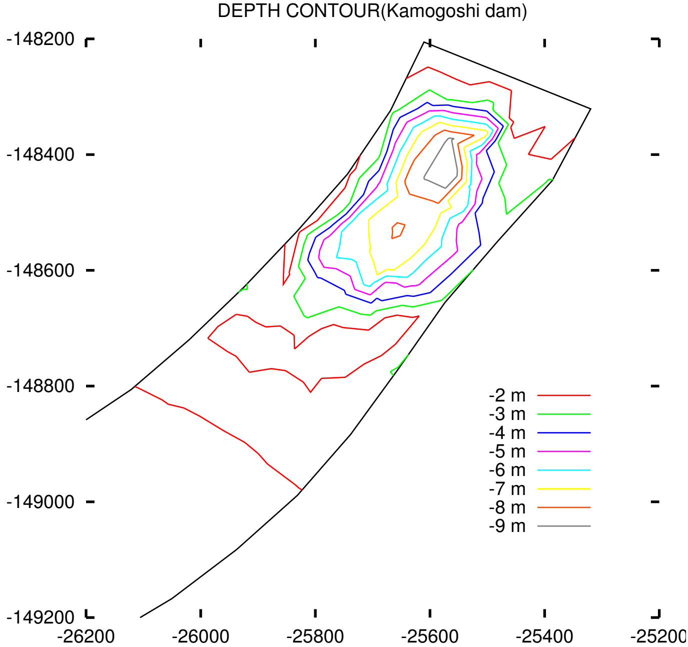

Figure 1: The depth contours in the region near the Kamogoshi Dam in the Yoshii River.

the depth of the river into a finite element analysis of equations that govern the dynamics of the currents. Experimental techniques to utilize the GPS in analyses of currents are also introduced. Figure 2 (based on the water level data of the river policy information of the Ministry of Land, Infrastructure, Transport and Tourism) shows the change of water levels of the the Yoshii River in the region near the Kamogoshii Dam and Kuban. The level rises and falls twice each day near the Kuban, because the Yoshii River is connected to the Seto Inland Sea. We study the lowest water levels from 13:00 to 16:00 JST, on July 23, 2010. Section 2 shows how the system of partial differential equations is solved by the finite element method. Section 3 applies this method to simulate the flow in the Yoshii River downstream from the

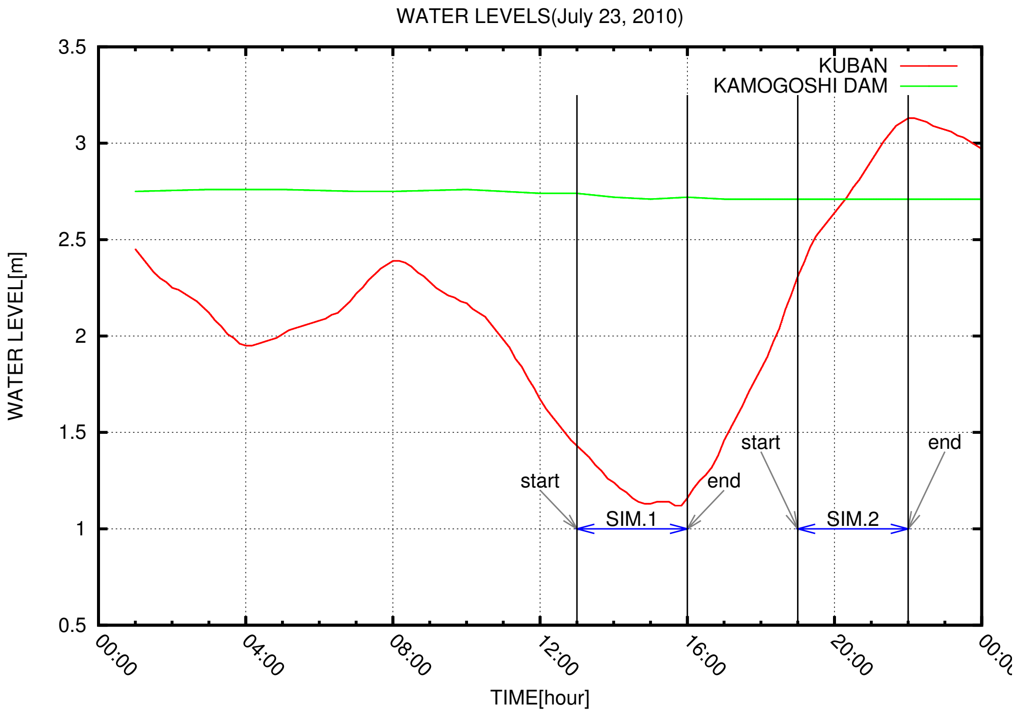

Figure 2: Change of water levels on July 23, 2010.

Kamogoshi Dam. The difference between simulation results using three layers and five layers is obtained, and the results are discussed in the Conclusion. Numerical simulations such as these are useful for studying the water quality of a river, and for analyzing the effects of a red tide.

2 Numerical solution by the finite element method

2.1 Shallow water equations

We apply a finite element method to Equations (1), (2), (3) and (4) to analyze the current generated in the Yoshii River. The shallow water equations consist of momentum equations and a continuity equation [1, 2, 3, 4], and model water in the river,

$$\frac{\partial u}{\partial t} + \frac{\partial (uu)}{\partial x} + \frac{\partial (uv)}{\partial y} + \frac{\partial (uw)}{\partial z} - fv + \frac{1}{\rho}\frac{\partial p}{\partial x} - \frac{1}{\rho}\left(\frac{\partial \tau_{xx}}{\partial x} + \frac{\partial \tau_{xy}}{\partial y} + \frac{\partial \tau_{xz}}{\partial z}\right) = 0\,, \tag{1}$$

$$\frac{\partial v}{\partial t} + \frac{\partial (vu)}{\partial x} + \frac{\partial (vv)}{\partial y} + \frac{\partial (vw)}{\partial z} + fu + \frac{1}{\rho}\frac{\partial p}{\partial y} - \frac{1}{\rho}\left(\frac{\partial \tau_{yx}}{\partial x} + \frac{\partial \tau_{yy}}{\partial y} + \frac{\partial \tau_{yz}}{\partial z}\right) = 0\,, \tag{2}$$

$$\frac{\partial w}{\partial t} + \frac{\partial (wu)}{\partial x} + \frac{\partial (wv)}{\partial y} + \frac{\partial (ww)}{\partial z} + \frac{1}{\rho}\frac{\partial p}{\partial z} - \frac{1}{\rho}\left(\frac{\partial \tau_{zx}}{\partial x} + \frac{\partial \tau_{zy}}{\partial y} + \frac{\partial \tau_{zz}}{\partial z}\right) + g = 0\,, \tag{3}$$

$$\frac{\partial u}{\partial x} + \frac{\partial v}{\partial y} + \frac{\partial w}{\partial z} = 0. \tag{4}$$

Here, the components of the stress tensor are

$$\tau_{xx} = -p + \mu\frac{\partial u}{\partial x}\,, \quad \tau_{yy} = -p + \mu\frac{\partial v}{\partial y}\,, \quad \tau_{zz} = -p + \mu\frac{\partial w}{\partial z}\,, \tag{5}$$

$$\tau_{xy} = \tau_{yx} = \frac{\mu}{2}\left(\frac{\partial u}{\partial y} + \frac{\partial v}{\partial x}\right), \quad \tau_{xz} = \tau_{zx} = \frac{\mu}{2}\left(\frac{\partial u}{\partial z} + \frac{\partial w}{\partial x}\right), \tag{6}$$

$$\tau_{yz} = \tau_{zy} = \frac{\mu}{2}\left(\frac{\partial v}{\partial y} + \frac{\partial w}{\partial x}\right), \tag{7}$$

and we use the following notation:

- x, y, z Cartesian coordinates positive eastward, northward, and upward, respectively;
- u, v, w respective components of velocity;
- t time;
- f Coriolis parameter;
- p pressure;
- $\rho = 1000\,\text{kg/m}^3$ is the density of water;
- μ viscosity coefficient of fluid;
- g gravitational acceleration;
- $\tau_{xx}, \tau_{xy}, \tau_{yx}, \tau_{yy}, \tau_{xz}, \tau_{yz}$ components of the stress tensor.

2.2 Initial condition

We also define the parameter $\gamma^2 = 0.0026$ to be a bottom friction coefficient [5] and A_h to be a constant that represents eddy viscosity. We set $A_h = 1.0$ for the results obtained on July 23, 2010. The governing equations for the mass and momentum are integrated over the kth layer, where $k = 1, 2, 3, \ldots, b$. Let

$$\langle\ \rangle_k = \int_{k+\frac{1}{2}}^{k-\frac{1}{2}} (\ )\,dz \tag{8}$$

where $k \pm \frac{1}{2}$ refers to z-levels of the interfaces between layers k and $k \pm 1$. Water fluxes M_k and N_k are obtained by integrating the x-component and the y-component of the velocity over the depth, respectively:

$$M_k = h_k u_k\,, \quad N_k = h_k v_k\,. \tag{9}$$

Along the curve

$$\frac{dx}{dt} = u_k\,, \quad \frac{dy}{dt} = v_k\,, \tag{10}$$

Equations (1) and (2) become

$$\begin{aligned}\frac{dM_k}{dt} &= \sum_{l=k}^{b}\left(\frac{\partial M_l}{\partial x}+\frac{\partial N_l}{\partial y}\right)\frac{1}{2}\left(\frac{M_{k-1}}{h_{k-1}}+\frac{M_k}{h_k}\right)\\ &\quad-\sum_{l=k+1}^{b}\left(\frac{\partial M_l}{\partial x}+\frac{\partial N_l}{\partial y}\right)\frac{1}{2}\left(\frac{M_k}{h_k}+\frac{M_{k+1}}{h_{k+1}}\right)-gh_k\frac{\partial \zeta}{\partial x}\\ &\quad-\gamma^2(\Delta V)_k\left(\frac{M_k}{h_k}-\frac{M_{k+1}}{h_{k+1}}\right)+\gamma^2(\Delta V)_{k-1}\left(\frac{M_{k-1}}{h_{k-1}}-\frac{M_k}{h_k}\right)\\ &\quad+\frac{A_h}{\rho}\frac{\partial^2 M_k}{\partial x^2}+\frac{A_h}{\rho}\frac{\partial^2 M_k}{\partial y^2},\end{aligned} \tag{11}$$

and

$$\begin{aligned}\frac{dN_k}{dt} &= \sum_{l=k}^{b}\left(\frac{\partial M_l}{\partial x}+\frac{\partial N_l}{\partial y}\right)\frac{1}{2}\left(\frac{N_{k-1}}{h_{k-1}}+\frac{N_k}{h_k}\right)\\ &\quad-\sum_{l=k+1}^{b}\left(\frac{\partial M_l}{\partial x}+\frac{\partial N_l}{\partial y}\right)\frac{1}{2}\left(\frac{N_k}{h_k}+\frac{N_{k+1}}{h_{k+1}}\right)-gh_k\frac{\partial \zeta}{\partial y}\\ &\quad-\gamma^2(\Delta V)_k\left(\frac{N_k}{h_k}-\frac{N_{k+1}}{h_{k+1}}\right)+\gamma^2(\Delta V)_{k-1}\left(\frac{N_{k-1}}{h_{k-1}}-\frac{N_k}{h_k}\right)\\ &\quad+\frac{A_h}{\rho}\frac{\partial^2 N_k}{\partial x^2}+\frac{A_h}{\rho}\frac{\partial^2 N_k}{\partial y^2},\end{aligned} \tag{12}$$

where

$$\begin{aligned}(\Delta V)_{k-1} &= \sqrt{(u_{k-1}-u_k)^2+(v_{k-1}-v_k)^2}\\ &= \sqrt{\left(\frac{M_{k-1}}{h_{k-1}}-\frac{M_k}{h_k}\right)^2+\left(\frac{N_{k-1}}{h_{k-1}}-\frac{N_k}{h_k}\right)^2}.\end{aligned} \tag{13}$$

At the rigid boundaries the values of M_k and N_k are set to zero. Initial conditions are given as $M_k = 0$ and $N_k = 0$ at all node points, where

$k = 1, 2, 3, \ldots, b$ and b is the total number of layers. A finite element method is applied to the Equations (1), (2), (3), and (4) to simulate the flow generated downstream from the Kamogoshi Dam, with a mesh consisting of 1798 elements and 965 nodes. Figure 3(a) shows the finite element mesh in the entire region of the Yoshii River Mouth. Figure 3(b) shows the finite element mesh in the region near the Kamogoshi Dam. Figures 4 shows a 3D view of this finite element mesh.

2.3 Application to the multi-layer finite element method

After multiplying the equation (11) by δM, we integrate over a domain Ω and obtain [6, 7, 8]

$$\begin{aligned}
\iint_\Omega \frac{\partial M_k}{\partial t}\delta M\,dx\,dy &= \frac{1}{2}\iint_\Omega \sum_{l=k}^{b}\left(\frac{\partial M_l}{\partial x}+\frac{\partial N_l}{\partial y}\right)\left(\frac{M_{k-1}}{h_{k-1}}+\frac{M_k}{h_k}\right)\delta M\,dx\,dy \\
&\quad -\frac{1}{2}\iint_\Omega \sum_{l=k+1}^{b}\left(\frac{\partial M_l}{\partial x}+\frac{\partial N_l}{\partial y}\right)\left(\frac{M_k}{h_k}+\frac{M_{k+1}}{h_{k+1}}\right)\delta M\,dx\,dy \\
&\quad -\iint_\Omega g h_k\frac{\partial \zeta}{\partial x}\delta M\,dx\,dy \\
&\quad -\iint_\Omega \gamma^2(\Delta V)_k\left(\frac{M_k}{h_k}-\frac{M_{k+1}}{h_{k+1}}\right)\delta M\,dx\,dy \\
&\quad +\iint_\Omega \gamma^2(\Delta V)_{k-1}\left(\frac{M_{k-1}}{h_{k-1}}-\frac{M_k}{h_k}\right)\delta M\,dx\,dy \\
&\quad +\iint_\Omega \frac{A_h}{\rho}\frac{\partial^2 M_k}{\partial x^2}\delta M\,dx\,dy \\
&\quad +\iint_\Omega \frac{A_h}{\rho}\frac{\partial^2 M_k}{\partial y^2}\delta M\,dx\,dy. \qquad (14)
\end{aligned}$$

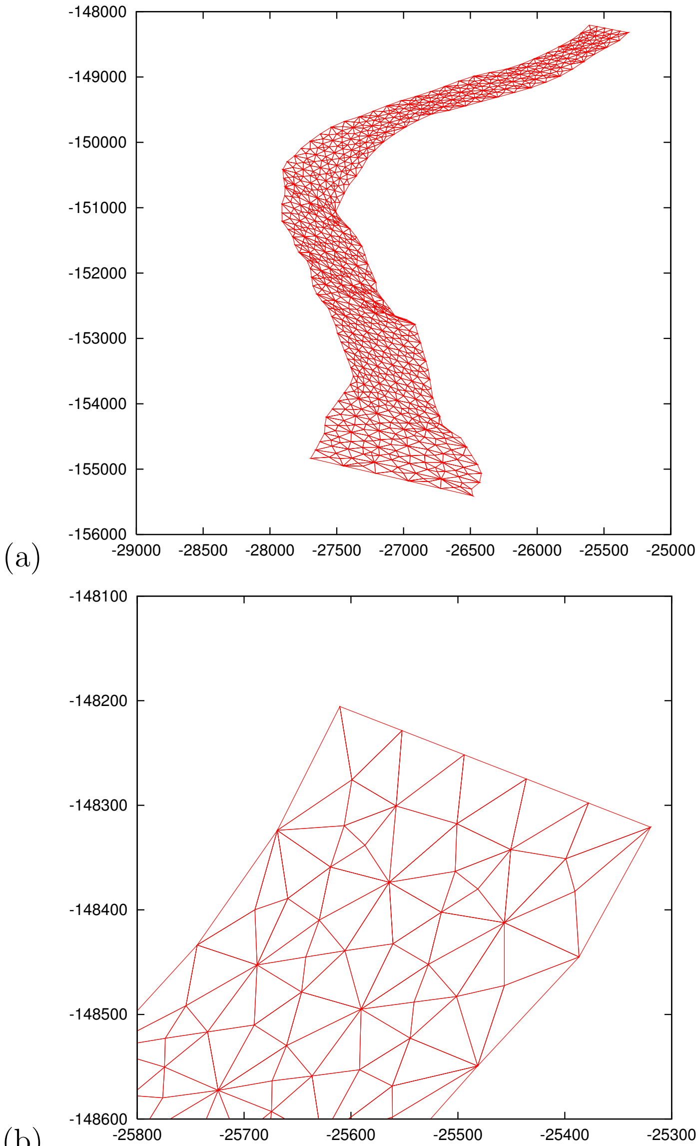

Figure 3: Finite element mesh consisting of 1798 elements and 965 nodes (a) in the entire region and (b) in the region near the Kamogoshi Dam.

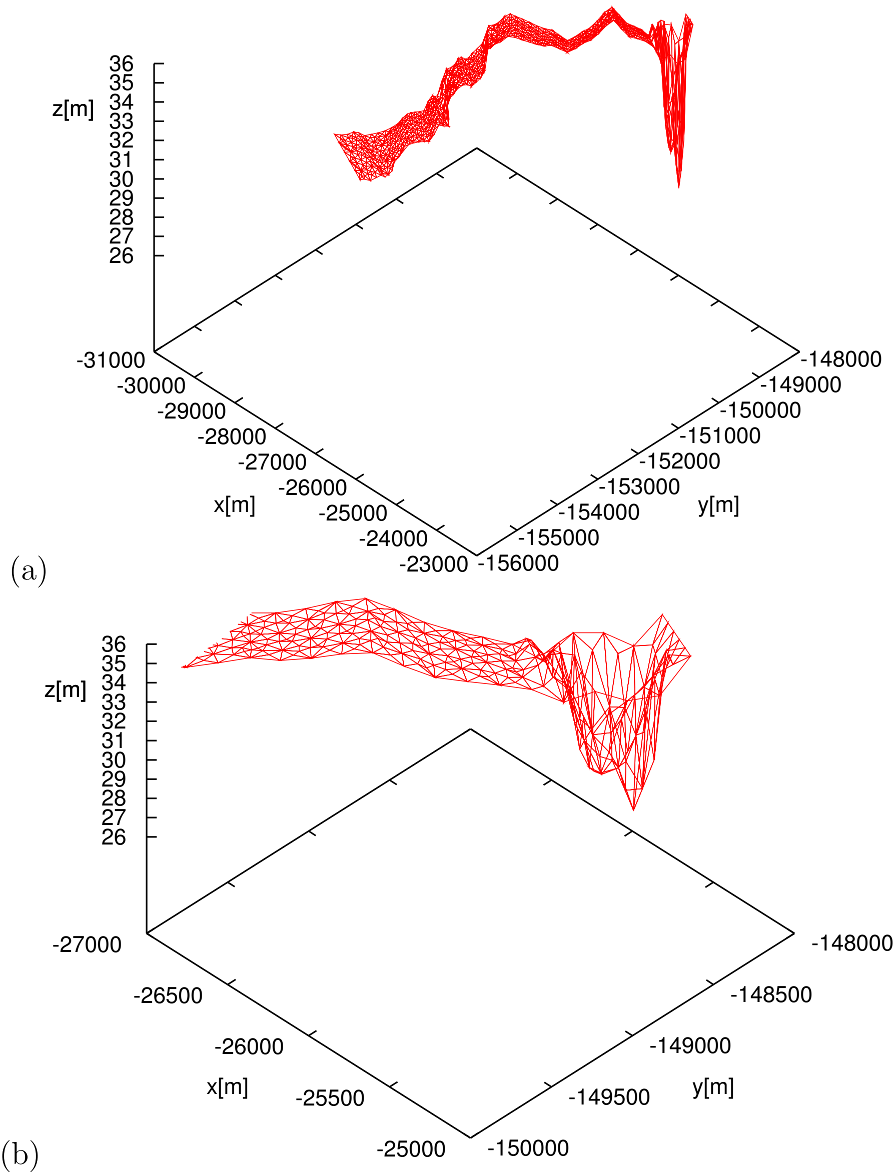

Figure 4: The mesh in three dimensions.

Let

$$M_k = \sum_{j=1}^{m} \phi_j M_k^j \,, \quad N_k = \sum_{j=1}^{m} \phi_j N_k^j \,,$$
$$h_k = \sum_{j=1}^{m} \phi_j h_k^j \,, \quad \zeta = \sum_{j=1}^{m} \phi_j \zeta^j \,, \quad \delta M = \phi_i \,, \tag{15}$$

where $\phi_1, \phi_2, \ldots, \phi_m$ are basis functions, m is the number of nodes, $i, j = 1, 2, \ldots, m$, and $k = 1, 2, \ldots, b$, where b is the number of layers. Applying Green's theorem and the approximations (15) to Equation (14), and dividing Ω into its constituent finite elements,

$$\begin{aligned}
&\sum_{j=1}^{m} \frac{\partial M_k^j}{\partial t} \sum_{\triangle} \iint_{\triangle} \phi_i \phi_j \, dx \, dy \\
&- \frac{1}{2} \sum_{l=k}^{b} \sum_{j=1}^{m} M_l^j \left\{ \sum_{\triangle} \iint_{\triangle} \left\{ \frac{\sum_{j=1}^{m} M_{k-1}^j \phi_j}{\sum_{j=1}^{m} h_{k-1}^j \phi_j} + \frac{\sum_{j=1}^{m} M_k^j \phi_j}{\sum_{j=1}^{m} h_k^j \phi_j} \right\} \frac{\partial \phi_j}{\partial x} \phi_i \, dx \, dy \right\} \\
&- \frac{1}{2} \sum_{l=k}^{b} \sum_{j=1}^{m} N_l^j \left\{ \sum_{\triangle} \iint_{\triangle} \left\{ \frac{\sum_{j=1}^{m} M_{k-1}^j \phi_j}{\sum_{j=1}^{m} h_{k-1}^j \phi_j} + \frac{\sum_{j=1}^{m} M_k^j \phi_j}{\sum_{j=1}^{m} h_k^j \phi_j} \right\} \frac{\partial \phi_j}{\partial y} \phi_i \, dx \, dy \right\} \\
&+ \frac{1}{2} \sum_{l=k+1}^{b} \sum_{j=1}^{m} M_l^j \left\{ \sum_{\triangle} \iint_{\triangle} \left\{ \frac{\sum_{j=1}^{m} M_k^j \phi_j}{\sum_{j=1}^{m} h_k^j \phi_j} + \frac{\sum_{j=1}^{m} M_{k+1}^j \phi_j}{\sum_{j=1}^{m} h_{k+1}^j \phi_j} \right\} \frac{\partial \phi_j}{\partial x} \phi_i \, dx \, dy \right\} \\
&+ \frac{1}{2} \sum_{l=k+1}^{b} \sum_{j=1}^{m} N_l^j \left\{ \sum_{\triangle} \iint_{\triangle} \left\{ \frac{\sum_{j=1}^{m} M_k^j \phi_j}{\sum_{j=1}^{m} h_k^j \phi_j} + \frac{\sum_{j=1}^{m} M_{k+1}^j \phi_j}{\sum_{j=1}^{m} h_{k+1}^j \phi_j} \right\} \frac{\partial \phi_j}{\partial y} \phi_i \, dx \, dy \right\} \\
&+ g \sum_{j=1}^{m} \zeta^j \left\{ \sum_{\triangle} \iint_{\triangle} \left(\sum_{q=1}^{m} h_k^q \phi_q \right) \left(\frac{\partial \phi_j}{\partial x} \phi_i \right) \, dx \, dy \right\} \\
&+ \gamma^2 \sum_{\triangle} \iint_{\triangle} (\Delta V)_k \left(\frac{\sum_{j=1}^{m} M_k^j \phi_j}{\sum_{j=1}^{m} h_k^j \phi_j} - \frac{\sum_{j=1}^{m} M_{k+1}^j \phi_j}{\sum_{j=1}^{m} h_{k+1}^j \phi_j} \right) \phi_i \, dx \, dy
\end{aligned}$$

$$-\gamma^2 \sum_{\triangle} \iint_{\triangle} (\Delta V)_{k-1} \left(\frac{\sum_{j=1}^{m} M_{k-1}^{j} \phi_j}{\sum_{j=1}^{m} h_{k-1}^{j} \phi_j} - \frac{\sum_{j=1}^{m} M_{k}^{j} \phi_j}{\sum_{j=1}^{m} h_{k}^{j} \phi_j} \right) \phi_i \, dx \, dy$$
$$+ \frac{A_h}{\rho} \sum_{j=1}^{m} M_k^j \left\{ \sum_{\triangle} \iint_{\triangle} \left(\frac{\partial \phi_j}{\partial x} \frac{\partial \phi_i}{\partial x} + \frac{\partial \phi_j}{\partial y} \frac{\partial \phi_i}{\partial y} \right) dx \, dy \right\} = 0 \,. \tag{16}$$

In the same way we obtain an equation for N_k. When the integration is carried out in each element, $\sum_{j=1}^{m} M_k^j \phi_j$, $\sum_{j=1}^{m} N_k^j \phi_j$, $\sum_{j=1}^{m} h_k^j \phi_j$ are replaced with their element averages $\bar{M}_{k_\triangle}, \bar{N}_{k_\triangle}$ and $\bar{h}_{k_\triangle}$. For example, in the second sum we approximate the integral over $\triangle$ by

$$\iint_{\triangle} \left\{ \frac{\bar{M}_{k-1_\triangle}}{\bar{h}_{k-1_\triangle}} + \frac{\bar{M}_{k_\triangle}}{\bar{h}_{k_\triangle}} \right\} \left(\frac{\partial \phi_j}{\partial x} \phi_i \right) dx \, dy \,.$$

Let

$$A_{ij} = \sum_{\triangle} \iint_{\triangle} \phi_i \phi_j \, dx \, dy \,,$$
$$B_{ij} = \sum_{\triangle} \iint_{\triangle} \frac{\partial \phi_j}{\partial x} \phi_i \, dx \, dy \,,$$
$$C_{ij} = \sum_{\triangle} \iint_{\triangle} \frac{\partial \phi_j}{\partial y} \phi_i \, dx \, dy \,,$$
$$D_{ij} = \sum_{\triangle} \iint_{\triangle} \left(\frac{\partial \phi_j}{\partial x} \frac{\partial \phi_i}{\partial x} + \frac{\partial \phi_j}{\partial y} \frac{\partial \phi_i}{\partial y} \right) dx \, dy \,,$$
$$B'_{k_{ij}} = \begin{cases} \sum_{\triangle} \frac{\bar{M}_{k_\triangle}}{\bar{h}_{k_\triangle}} \iint_{\triangle} \frac{\partial \phi_j}{\partial x} \phi_i \, dx \, dy & (k = 1) \\ \sum_{\triangle} \left\{ \frac{\bar{M}_{k-1_\triangle}}{\bar{h}_{k-1_\triangle}} + \frac{\bar{M}_{k_\triangle}}{\bar{h}_{k_\triangle}} \right\} \iint_{\triangle} \frac{\partial \phi_j}{\partial x} \phi_i \, dx \, dy & (k = 2, 3, \ldots), \end{cases}$$
$$C'_{k_{ij}} = \begin{cases} \sum_{\triangle} \frac{\bar{M}_{k_\triangle}}{\bar{h}_{k_\triangle}} \iint_{\triangle} \frac{\partial \phi_j}{\partial y} \phi_i \, dx \, dy & (k = 1) \\ \sum_{\triangle} \left\{ \frac{\bar{M}_{k-1_\triangle}}{\bar{h}_{k-1_\triangle}} + \frac{\bar{M}_{k_\triangle}}{\bar{h}_{k_\triangle}} \right\} \iint_{\triangle} \frac{\partial \phi_j}{\partial y} \phi_i \, dx \, dy & (k = 2, 3, \ldots), \end{cases}$$

$$F_{k_{ij}} = \sum_{\triangle} \bar{h}_{k_\triangle} \iint_\triangle \frac{\partial \phi_j}{\partial x} \phi_i \, dx\, dy \,,$$

$$G_{k_{ij}} = \begin{cases} \sum_\triangle \frac{\Delta \bar{V}_{k-1_\triangle}}{\bar{h}_{k-1_\triangle}} \iint_\triangle \phi_i \phi_j \, dx\, dy & (k = 2, 3, \ldots) \\ 0 & (k = 1), \end{cases}$$

$$H_{k_{ij}} = \begin{cases} \sum_\triangle \frac{\Delta \bar{V}_{k_\triangle}}{\bar{h}_{k+1_\triangle}} \iint_\triangle \phi_i \phi_j \, dx\, dy & (k = 1, 2, \ldots, b-1) \\ 0 & (k = b), \end{cases}$$

$$I_{k_{ij}} = \begin{cases} \sum_\triangle \frac{\Delta \bar{V}_{k_\triangle}}{\bar{h}_{k_\triangle}} \iint_\triangle \phi_i \phi_j \, dx\, dy & (k = 1) \\ \sum_\triangle \frac{\Delta \bar{V}_{k-1_\triangle} + \Delta \bar{V}_{k_\triangle}}{\bar{h}_{k_\triangle}} \iint_\triangle \phi_i \phi_j \, dx\, dy & (k = 2, 3, \ldots), \end{cases}$$

$$Q'_{k_{ij}} = \begin{cases} \sum_\triangle \frac{\bar{N}_{k_\triangle}}{\bar{h}_{k_\triangle}} \iint_\triangle \frac{\partial \phi_j}{\partial x} \phi_i \, dx\, dy & (k = 1) \\ \sum_\triangle \left\{ \frac{\bar{N}_{k-1_\triangle}}{\bar{h}_{k-1_\triangle}} + \frac{\bar{N}_{k_\triangle}}{\bar{h}_{k_\triangle}} \right\} \iint_\triangle \frac{\partial \phi_j}{\partial x} \phi_i \, dx\, dy & (k = 2, 3, \ldots), \end{cases}$$

$$P'_{k_{ij}} = \begin{cases} \sum_\triangle \frac{\bar{N}_{k_\triangle}}{\bar{h}_{k_\triangle}} \iint_\triangle \frac{\partial \phi_j}{\partial y} \phi_i \, dx\, dy & (k = 1) \\ \sum_\triangle \left\{ \frac{\bar{N}_{k-1_\triangle}}{\bar{h}_{k-1_\triangle}} + \frac{\bar{N}_{k_\triangle}}{\bar{h}_{k_\triangle}} \right\} \iint_\triangle \frac{\partial \phi_j}{\partial y} \phi_i \, dx\, dy & (k = 2, 3, \ldots). \end{cases}$$

Working with the element averages in this way, we approximate (16) by

$$A \frac{\partial M_k}{\partial t} + \frac{A_h}{\rho} M_k D - \frac{1}{2} \sum_{l=k}^{b} (M_l B'_k + N_l C'_k) + \frac{1}{2} \sum_{l=k+1}^{b} \left(M_l B'_{k+1} + N_l C'_{k+1} \right) + g\zeta F_k - \gamma^2 \left(M_{k-1} G_k - M_k I_k + M_{k+1} H_k \right) = 0 \,. \tag{17}$$

The momentum equation (12) becomes

$$A \frac{\partial N_k}{\partial t} + \frac{A_h}{\rho} N_k D - \frac{1}{2} \sum_{l=k}^{b} (M_l Q'_k + N_l P'_k) + \frac{1}{2} \sum_{l=k+1}^{b} \left(M_l Q'_{k+1} + N_l P'_{k+1} \right) + g\zeta F_k - \gamma^2 \left(N_{k-1} G_k - N_k I_k + N_{k+1} H_k \right) = 0 \,, \tag{18}$$

and the continuity equation (4) becomes

$$A\frac{\partial\zeta}{\partial t}+\sum_{l=1}^{b}\left(BM_l+CN_l\right)=0\,, \qquad (19)$$

where b is the number of layers.

2.4 Time-step approximation

For a given M_l^t, N_l^t and ζ^t, we calculate ζ^{t+1}, where t and $t+1$ denote the consecutive time steps. The continuity equation (19) becomes

$$A_{ij}\frac{\zeta_j^{t+1}-\zeta_j^t}{\Delta t}=-\sum_{l=1}^{n}\left\{B_{ij}\left(M_l\right)_j^t+C_{ij}\left(N_l\right)_j^t\right\}, \qquad (20)$$

implying that

$$A_{ij}\zeta_j^{t+1}=-\Delta t\sum_{l=1}^{n}\left\{B_{ij}\left(M_l\right)_j^t+C_{ij}\left(N_l\right)_j^t\right\}+A_{ij}\zeta_j^t\,. \qquad (21)$$

Putting $-\Delta t\sum_{l=1}^{n}\left\{B_{ij}\left(M_l\right)_j^t+C_{ij}\left(N_l\right)_j^t\right\}+A_{ij}\zeta_j^t=p_{3_i}$ and letting A_3 denote the matrix with entries A_{ij}, then ζ^{t+1} is obtained as the solution of the linear system

$$A_3\zeta^{t+1}=p_3\,. \qquad (22)$$

For given values of M_j^t, N_j^t, ζ_j^t and ζ_j^{t+1} we calculate the values of M_j^{t+1} and N_j^{t+1} using the discrete-time form of the momentum equation (17),

$$\begin{aligned}&\sum_j A_{ij}\frac{\left(M_k\right)_j^{t+1}-\left(M_k\right)_j^t}{\Delta t}\\&=-\frac{A_h}{\rho}\sum_j\left[\left(1-\theta\right)\left(M_k\right)_j^t+\theta\left(M_k\right)_j^{t+1}\right]D_{ij}\end{aligned}$$

$$+\frac{1}{2}\sum_{l=k}^{b}\sum_{j}\left\{(B'_k)_{ij}(M_l)_j^t+(C'_k)_{ij}(N_l)_j^t\right\}$$
$$-\frac{1}{2}\sum_{l=k+1}^{b}\left\{\left(B'_{k+1}\right)_{ij}(M_l)_j^t+\left(C'_{k+1}\right)_{ij}(N_l)_j^t\right\}$$
$$-g\sum_{j}\left[(1-\theta)\zeta_{j_*}^t+\theta\zeta_j^{t+1}\right](F_k)_{ij}$$
$$+\gamma^2\sum_{j}\left\{(M_{k-1})_j^t(G_k)_{ij}-(M_k)_j^t(I_k)_{ij}+(M_{k+1})_j^t(H_k)_{ij}\right\}. \tag{23}$$

The above equation is written as

$$\sum_{j}\left[A_{ij}+\Delta t\frac{A_h}{\rho}\theta D_{ij}\right](M_k)_j^{t+1}$$
$$=\sum_{j}\left\{A_{ij}-\Delta t\frac{A_h}{\rho}(1-\theta)D_{ij}\right\}(M_k)_j^t$$
$$+\frac{1}{2}\Delta t\sum_{l=k}^{b}\sum_{j}\left\{(B'_k)_{ij}(M_l)_j^t+(C'_k)_{ij}(N_l)_j^t\right\}$$
$$-\frac{1}{2}\Delta t\sum_{l=k+1}^{b}\left\{\left(B'_{k+1}\right)_{ij}(M_l)_j^t+\left(C'_{k+1}\right)_{ij}(N_l)_j^t\right\}$$
$$-\Delta t g\sum_{j}\left[(1-\theta)\zeta_{j_*}^t+\theta\zeta_j^{t+1}\right](F_k)_{ij}$$
$$+\Delta t\gamma^2\sum_{j}\left\{(M_{k-1})_j^t(G_k)_{ij}-(M_k)_j^t(I_k)_{ij}+(M_{k+1})_j^t(H_k)_{ij}\right\}. \tag{24}$$

Instead of calculating ζ_j^t, we calculate $\zeta_{j^*}^t$ at the point (x^*, y^*), where x^* and y^* are calculated from the system of ordinary differential equations

$$\frac{dx}{dt}=u\,,\quad \frac{dy}{dt}=v\,. \tag{25}$$

Thus,

$$x^* = x_j - \frac{M_j^t}{\zeta_j^t + h_j}\Delta t\,, \quad y^* = y_j - \frac{N_j^t}{\zeta_j^t + h_j}\Delta t\,. \tag{26}$$

We denote the right-hand side of Equation (24) by p_{1_i} and let A_1 denote the matrix with entries $A_{ij} + \Delta t\,(A_h/\rho)\theta D_{ij}$, then $(M_k)_j^{t+1}$ is the solution of the linear system

$$A_1 M_k^{t+1} = p_1\,. \tag{27}$$

Similarly, we obtain $(N_k)_j^{t+1}$ as the solution of the linear system

$$A_2 N_k^{t+1} = p_2\,. \tag{28}$$

Let a_{ij} be the entry in the ith row and the jth column of A_1. Suppose that the ith node is on the rigid boundary. We redefine $a_{ij} = \delta_{ij}$, and set the ith entry of p_1 to 0. For given M_k^t, M_k^{t+1}, N_k^t, N_k^{t+1} and ζ^t, we calculate ζ^{t+1}. The continuity equation (21) becomes

$$\begin{aligned}\sum_j A_{ij}\zeta_j^{t+1} = &-\Delta t\sum_{l=1}^{b}\sum_j\left\{(1-\theta)\,(M_l)_j^t + \theta\,(M_l)_j^{t+1}\right\}B_{ij}\\ &-\Delta t\sum_{l=1}^{n}\sum_j\left\{(1-\theta)\,(N_l)_j^t + \theta\,(N_l)_j^{t+1}\right\}C_{ij} + \sum_j A_{ij}\zeta_j^t\,.\end{aligned} \tag{29}$$

We denote the right-hand side of the equation (29) by p_3', then ζ_j^{t+1} is the solution of the simultaneous linear equation:

$$A_3\zeta^{t+1} = p_3'\,. \tag{30}$$

Let a_{ij} be the entry in the ith row and the jth column of A_3. Suppose that the ith node is on the open boundary. We redefine $a_{ij} = \delta_{ij}$, and set the ith entry of p_3 to the value of ζ_i^{t+1} given by the boundary conditions.

3 Flow simulation downstream of the Kamogoshi Dam

The finite element method was applied to Equations (1), (2), (3) and (4) to simulate the flow generated in the downstream region of the Kamogoshi Dam in Yoshii River. Simulations were conducted for three, five, seven and ten layers. The results for five, seven and ten layers are almost the same. When the total number of layers are three or five:

- Figure 5 shows velocity vectors at 15:00 JST ($t = 7200$ s after 13:00 JST), in the region near the Kamogoshi Dam for the bottom layer;
- Figure 6 shows velocity vectors at 15:00 JST in the region near the Yoshii River Mouth for the bottom layer;
- Figure 7 shows velocity vectors at 15:00 JST in the region near the Yoshii River Mouth for the middle layer;
- Figure 8 shows velocity vectors at 15:00 JST in the region near the Yoshii River Mouth for the surface layer.

The finite element mesh shown in Figure 3 was used.

4 Conclusion

The result of a simulation of the flow of the Yoshii River is shown. The three layer simulation results of the lowest water levels between 13:00 and 16:00 JST one day are presented. A reflux from the Yoshii River Mouth in the entire region at 15:00 JST is observed. A vortex occurs in the bottom layer in the deepest part near the Kamogoshi Dam. It is shown in both the three layer and the five layer results.

We introduced bathymetric data of our own, shown in Figure 1, into the

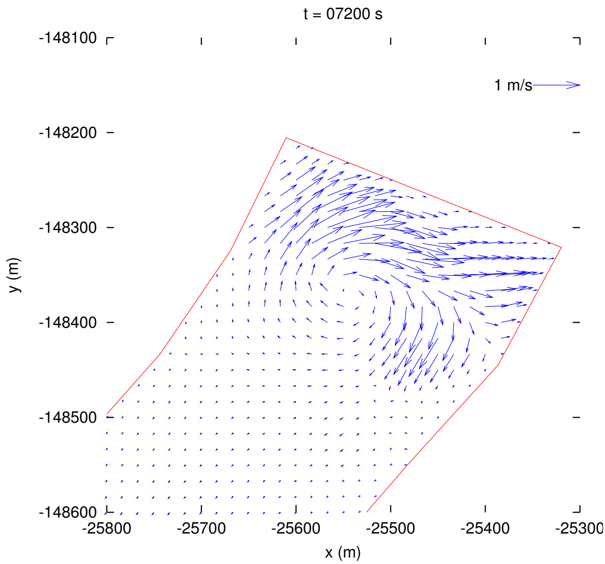

(a) three layer

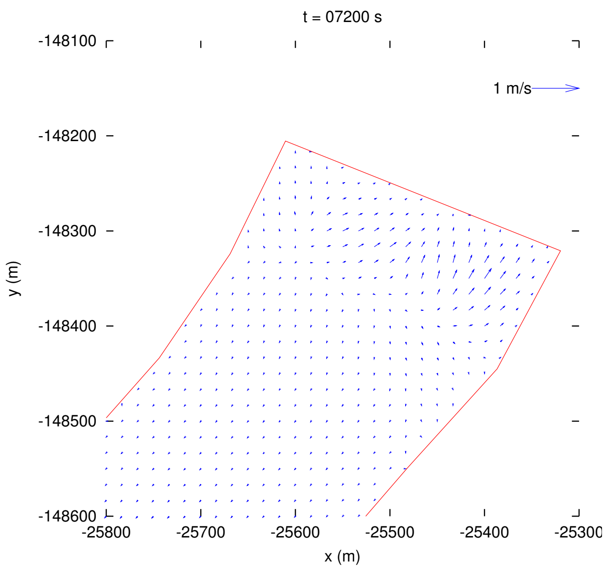

(b) five layer

Figure 5: Velocity vectors for the bottom layer in a region near the Kamogoshi Dam at 15:00 JST on July 23, 2010.

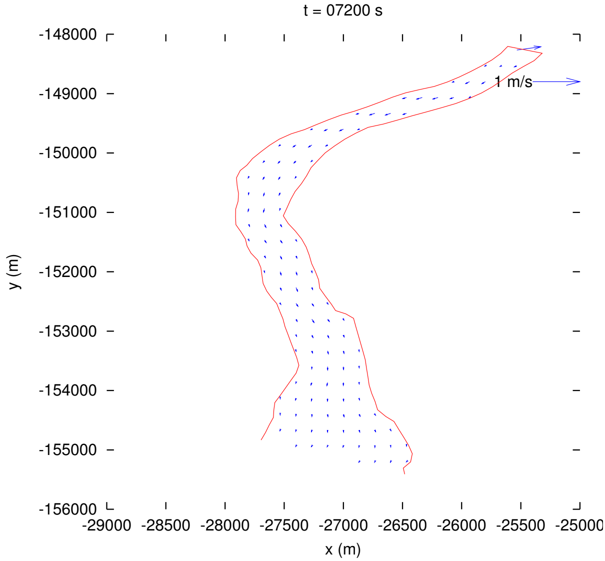

(a) three layer

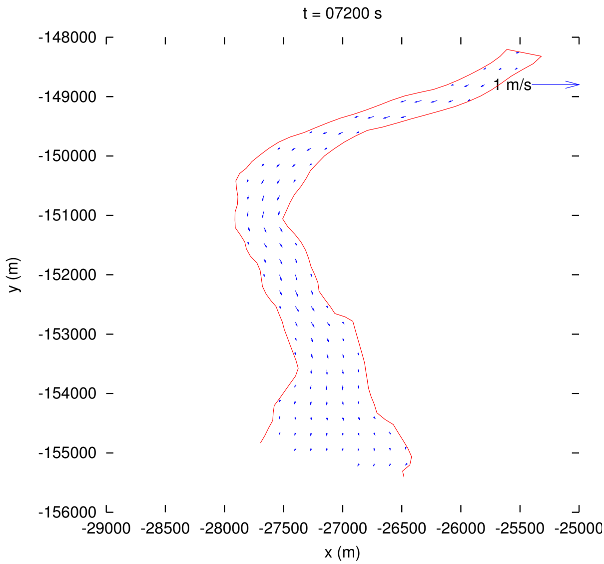

(b) five layer

Figure 6: Velocity vectors for the bottom layer in a region near the Yoshii River Mouth at 15:00 JST on July 23, 2010.

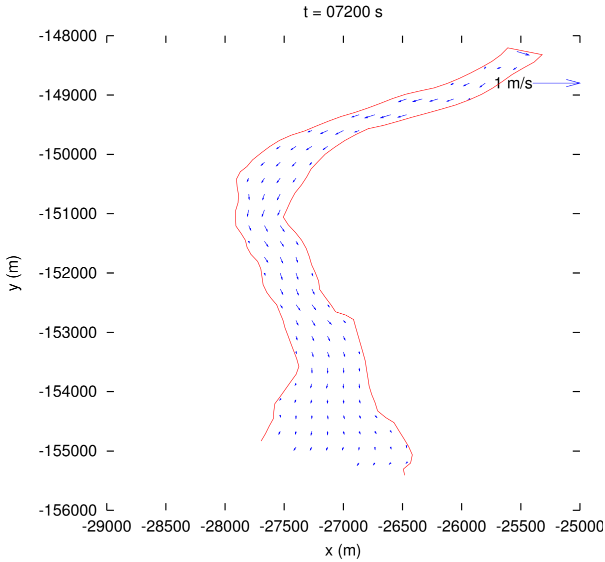

(a) three layer

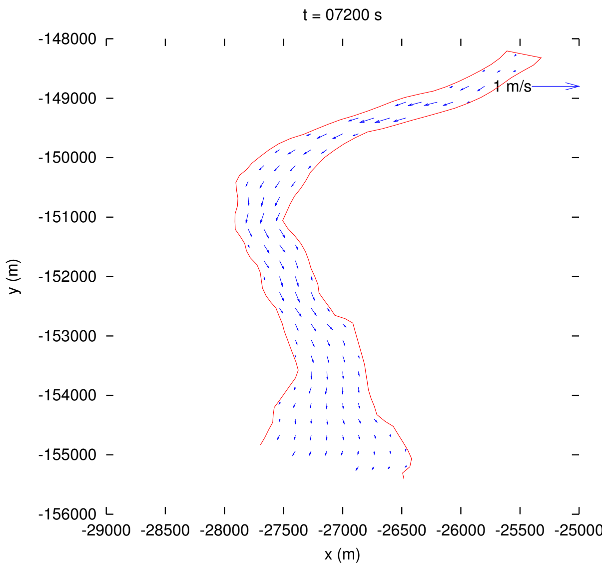

(b) five layer

Figure 7: Velocity vectors for the middle layer in a region near the Yoshii River Mouth at 15:00 JST on July 23, 2010.

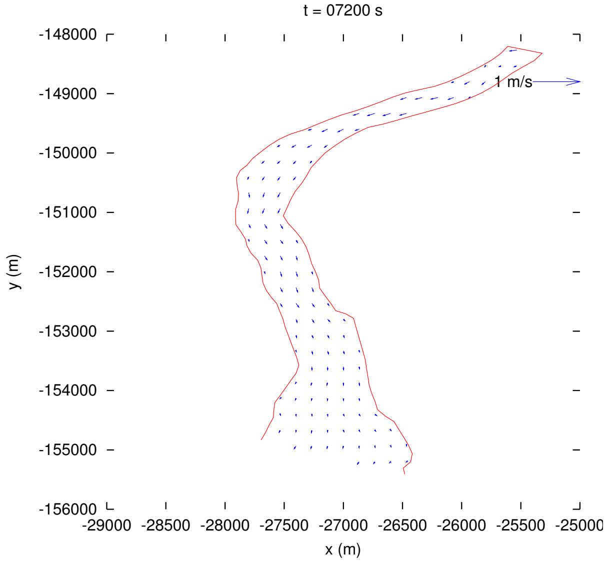

(a) three layer

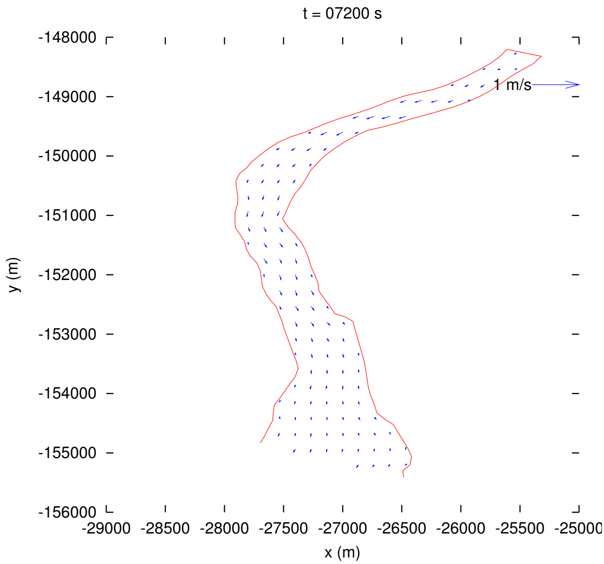

(b) five layer

Figure 8: Velocity vectors for the surface layer in a region near the Yoshii River Mouth at 15:00 JST on July 23, 2010.

analysis of the flow in the Yoshii River. Measurements were conducted using a RTK-GPS and a high precision echo sounder on a boat. The positioning data and the depth data were obtained along the trace of the boat. RTK-GPS data in terms of the latitude, the longitude, and the reference ellipsoidal height were obtained. The data were transformed to rectangular coordinates by Gauss–Grüger projection. Time-position data and time-depth data were synchronized, and the least squares approximation over each element was applied to generate the depth-position data shown in Figure 1. The numerical results demonstrate that our techniques for measurement and simulation are practically appropriate.

Acknowledgements The water level data was obtained from the river policy information of the Ministry of Land, Infrastructure, Transport and Tourism in Japan on July 23, 2010 [9]. The results concerning the bottom topography of the Yoshii River were obtained in research commissioned by the Okayama City "Study on water depth etc. downstream Kamogoshi Dam and vicinity in Yoshii River" in 2010.

References

[1] O. C. Zienkiewicz and R. L. Taylor, *The Finite Element Method, Volume 3, Fluid Dynamics*, Fifth Edition, Butterworth-Heinemann, Oxford, 2000 (First published in 1967 by McGraw-Hill). C1106

[2] R. G. Dean and R. A. Dalrymple, *Water Wave Mechanics for Engineers and Scientists*, Advanced Series on Ocean Engineering, Volume 2, World Scientific, Singapore, 1991. C1106

[3] M. Kawahara, M. Kobayashi, K. Nakata, Multiple level finite element analysis and its applications to tidal current flow in Tokyo Bay, *Appl. Math. Modelling*, Vol. 7, June 1983. C1106

[4] Jan J. Leendertse, Richard C. Alexander, Shiao-Kung Liu, *A three-dimensional model for estuaries and coastal seas: Volume I, Principles of computation*, R-1417-OWRR, December 1973 C1106

[5] Yoshiiaki Iwasa, *Engineering Limnology*, Sankaido Publishing Co., Ltd., 1990 (In Japanese) C1107

[6] Ying Liu, Kazuhiro Yamamoto, Majda Ceric, Masaji Watanabe, Numerical study of flow generated in a lake and experiment using GPS, Proceedings of the 14th Biennial Computational Techniques and Applications Conference. CTAC-2008, Editors: Geoffry N. Mercer and A. J . Roberts, *ANZIAM J.* vol. 50, pp.C912–C929, 2009. http://journal.austms.org.au/ojs/index.php/ANZIAMJ/article/view/1470 C1109

[7] Masaji Watanabe, A Numerical Simulation of Lake Flow and a GPS-Float Experiment, *The Second International Symposium on Water Environment*, Okayama University, September 13–14, 1999, Journal of the Faculty of Environmental Science and Technology, Okayama University (Special Edition), pp.111–116. C1109

[8] Masaji Watanabe, Ying Liu, Kazuhiro Yamamoto, Majda Ceric, Numerical study of flow generated in a lake and experimental technique for verification, *Proceedings of the 2nd International Symposium on Shallow Flows*, HKUST, Hong Kong, December 10–12, 2008. C1109

[9] http://www.mlit.go.jp/ C1123

Author addresses

1. **Hashentuya**, Graduate School of Environmental Science, Okayama University, Japan.
mailto:dev422252@s.okayama-u.ac.jp

2. **Yoji Otani**, Graduate School of Environmental Science, Okayama University, Japan.

mailto:gev421104@s.okayama-u.ac.jp

3. **Kazuhiro Yamamoto**, Graduate School of Environmental Science, Okayama University, Japan.
mailto:dev421102@s.okayama-u.ac.jp

4. **Masaji Watanabe**, Graduate School of Environmental Science, Okayama University, Japan.
mailto:watanabe@ems.okayama-u.ac.jp